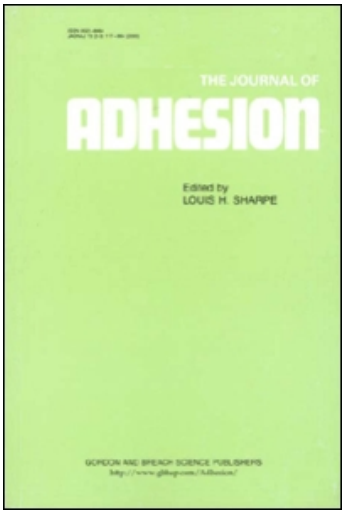

The Journal of Adhesion

Publication details, including instructions for authors and subscription information:
http://www.informaworld.com/smpp/title~content=t713453635

Three-dimensional Finite Element Analysis of Stress Response in Adhesive Butt Joints Subjected to Impact Tensile Loads

Izumi Higuchi[a]; Toshiyuki Sawa[b]; Hirohisa Okuno[c]
[a] Kofu High School of Technology, Kofu, Yamanashi, Japan [b] Dept. of Mechanical Engineering, Yamanashi University, Kofu, Yamanashi, Japan [c] Nippon Denso Co. Ltd, Yamanashi University, Japan

To cite this Article Higuchi, Izumi , Sawa, Toshiyuki and Okuno, Hirohisa(1999) 'Three-dimensional Finite Element Analysis of Stress Response in Adhesive Butt Joints Subjected to Impact Tensile Loads', The Journal of Adhesion, 69: 1, 59 — 82
To link to this Article: DOI: 10.1080/00218469908015919
URL: http://dx.doi.org/10.1080/00218469908015919

J. Adhesion, 1999, Vol. 69, pp. 59–82
Reprints available directly from the publisher
Photocopying permitted by license only

Three-dimensional Finite Element Analysis of Stress Response in Adhesive Butt Joints Subjected to Impact Tensile Loads*

IZUMI HIGUCHI[a], TOSHIYUKI SAWA[b,**] and HIROHISA OKUNO[c]

[a] *Kofu High School of Technology, Kofu, Yamanashi, 400 Japan;*
[b] *Dept. of Mechanical Engineering, Yamanashi University, 4-3-11, Takeda, Kofu, Yamanashi, 400 Japan;*
[c] *Yamanashi University, presently, Nippon Denso Co. Ltd., Japan*

(Received 12 November 1996; In final form 14 May 1998)

The stress wave propagation and the stress distribution in adhesive butt joints of similar adherends subjected to impact loads are analyzed using a three-dimensional finite-element method (FEM). The code employed is DYNA3D. An impact load is applied to a joint by dropping a weight. An adherend of a joint is fixed and the other adherend to which a bar is connected is impacted by the weight. The height of the weight is changed. The effect of Young's modulus ratio between the adherends and the adhesive, the adhesive thickness and the geometry of *T*-shaped adherends on the stress wave propagation at the interfaces are examined. It is found that the maximum stress is caused at the interfaces of the adherend subjected to an impact load. In the case of a *T*-shaped adherend, it is seen that the maximum stress is caused near the center of the interfaces and that it increases as Young's modulus of the adherends increases. In the special case where the web length of the *T*-shaped adherends equals the interface length, it is seen that the singular stress occurs at the edge of the interfaces and it increases as Young's modulus of the adherends decreases. The maximum principal stress increases as the adherend thickness increases. In addition, the strain response of adhesive butt joints subjected to impact loads was measured using strain gauges. A fairly good agreement is found between the numerical and the measured results.

Keywords: Elasticity; stress analysis; FEM; adhesive joints; impact loads; interface stress; three-dimensional; *T*-shaped flange; singular stress

*Presented at EURADH'96/ADHESION'96 (European Adhesion Conference), Churchill College, Cambridge, UK, 3–6 September, 1996.

**Corresponding author. Fax: +81-552-20-8438 (or -8779).

1. INTRODUCTION

Adhesive joints have been used in mechanical structures, automobile and aerospace industries, electrical devices and so on. Many researches [1–9] have been carried out on stress distributions in butt, lap and scarf adhesive joints subjected to static, repeated and thermal loads. Few researches [10–13] have been carried out on stress propagation and the stress distribution in adhesive joints subjected to impact loads. In practice, it is necessary to know the stress propagation and the stress distribution of adhesive joints subjected to impact loads from a design reliability standpoint. In this paper, the stress wave propagation and the stress distribution in adhesive butt joints of T-shaped similar adherends subjected to impact loads are analyzed using a three-dimensional finite-element method (FEM) [14]. The code employed is DYNA3D. An impact load is applied to a joint by dropping a weight. The analysis is performed in elastic deformation. One adherend of a joint is fixed and the other adherend to which a bar is connected is impacted by the weight. The height of the weight is changed. The effect of Young's modulus ratio between the adherends and the adhesive, the adhesive thickness and the geometry of T-shaped adherends on the stress wave propagation at the interfaces are examined. In addition, the strain response of joints subjected to an impact load was measured. The analytical results are compared with the measured results.

2. FINITE-ELEMENT ANALYSIS

Figure 1 shows a model for analysis of a T-shaped adhesive butt joint. The coordinate system (x, y, z) used is as shown in Figure 1. A pin is inserted into a hole of the lower adherend (Solid 3) and a circular plate is connected to the pin. A weight (Solid 4) is impacted on the circular plate. The height of adherends and the flange height of the T-shaped adherends are denoted by h_3 and h_1. The adhesive thickness, the thickness in the z-direction, the length of flange and the web length are denoted by h_2, $2w$, $2l_1$ and $2l_2$, respectively. Young's moduli and Poisson's ratio of the T-shaped adherends are denoted by E_1, ν_1 and those of an adhesive by E_2 and ν_2, respectively. Taking the symmetry

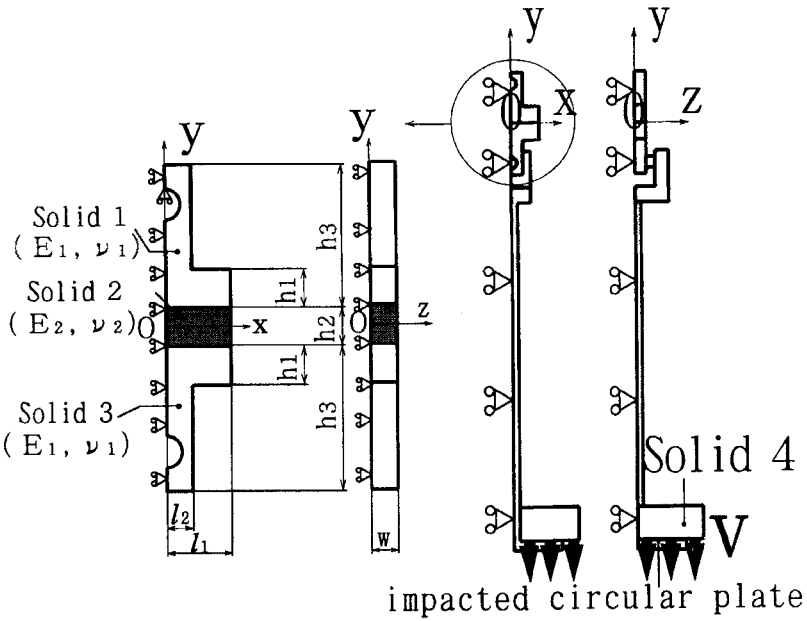

FIGURE 1 A model for analysis in the case of *T*-shaped adhesive butt joints.

of the joint to the axes $x = 0$ and $z = 0$ into consideration, one-quarter of the joint is analyzed as shown in Figure 1. The boundary conditions are as follows: the nodal points at $x = 0$ and $z = 0$ and the nodal point of the hole in the upper adherend (Solid 1) are fixed in the y direction, and an impact load is applied to the joint by providing an initial velocity, v, at the weight (Solid 4) as shown in Figure 1. Figure 2 shows an example of mesh division. Pentahedral and hexahedral elements [15] are used. The number of elements and nodes employed are 1508 and 2534. The finite element method [14] (code name is DYNA3D [16, 17]) employed is explicit and a three-dimensional elastic analysis is carried out.

In the code DYNA3D, the equation of motion is described using the principle of virtual work as the equation $[M][A] + [K][U] = [F]$, where $[M]$ is the mass matrix, $[A]$ is the acceleration vector, $[K]$ is the stiffness matrix, $[U]$ is the displacement vector, and $[F]$ is the external load vector. Taking into account the initial condition, boundary condition and the contact condition, the calculation in DYNA3D is

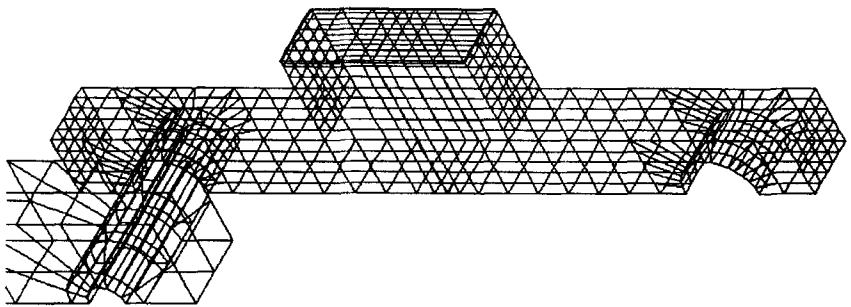

FIGURE 2 An example of element division in impact analysis of T-shaped joints.

carried out. In the initial condition, the condition $u(x, t) = u_1$ at $t = 0$ on some domain is usually used, where x is the position variable, u is the displacement, u_1 is the prescribed displacement and t is the time. However, in DYNA3D, the condition $du/dt(x, t) = v_1$ at $t = 0$ on some domain is used, where v_1 is the prescribed value of velocity. In addition, in DYNA3D, the time integration is done by using the center difference method.

Figure 3 shows a joint in the case where the web length, $2l_2$, is equal to the flange length $2l_1$ ($l_2 = l_1$ in Fig. 1). In the analysis, the computations are performed for the joint shown in Figure 3 in order to examine the effect of the web length on the interface stress distributions.

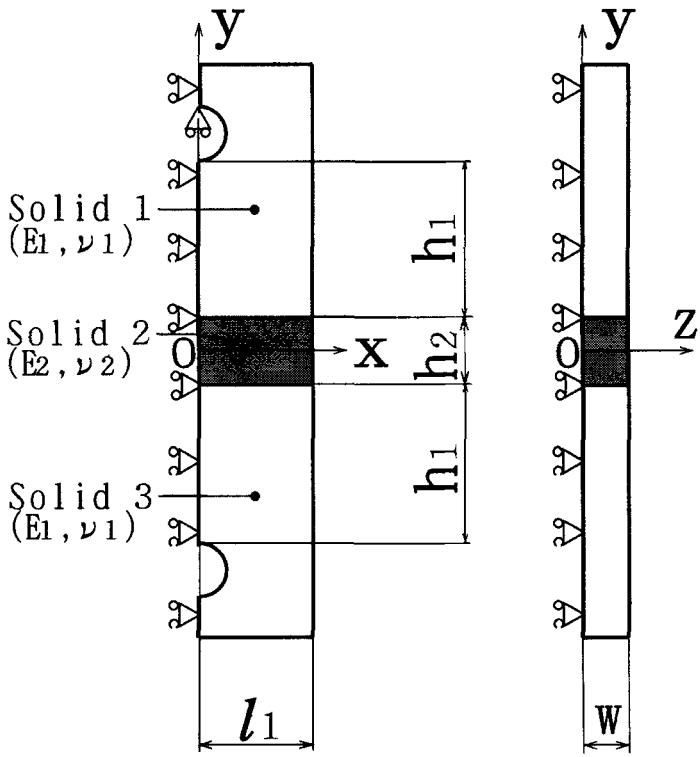

FIGURE 3 A model for analysis where web length $2l_2$ is equal to flange length $2l_1$.

3. EXPERIMENTAL METHOD

Figure 4 shows the dimensions of specimens used in the strain measurement. The specimens are joined by an epoxy adhesive [SUMITOMO 3M Co. Ltd. in Japan, Scotch-Weld 1838]. Figure 5 shows a schematic experimental setup and the positions of the attached strain gauges. The strain gauges are attached 2 mm from the interfaces and the positions are 0, 8, 12 and 16 mm from the center of the joint as shown in Figure 5. The joint was fixed using a 12 mm diameter pin and the weight of 26.754 N was dropped from the height of $H = 500$ mm. The strain responses were recorded using an analyzing recorder the resolution of which is better than 1 μs (1×10^{-6} second). The length of the connected bar from the impacted circular plate to the pin of the lower adherend shown in Figure 1 is 1370 mm.

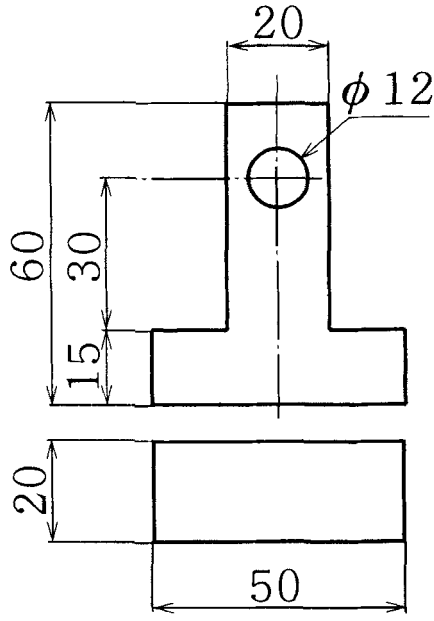

FIGURE 4 Dimensions of specimen used in the experiment.

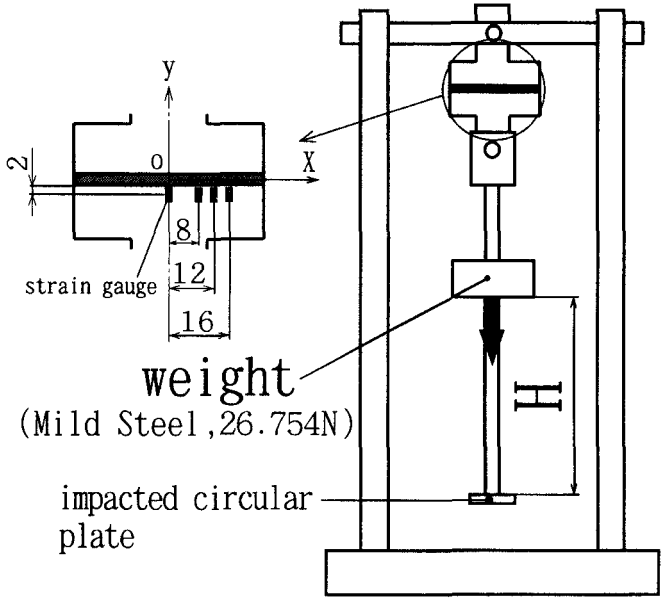

FIGURE 5 A schematic experimental setup for measuring strain response.

4. RESULTS OF ANALYSIS AND THE COMPARISONS BETWEEN THE ANALYTICAL AND THE MEASURED RESULTS

4.1. Results of Analysis

In the numerical calculations, the dimensions of the specimens used are the same as those used in the strain measurements (Fig. 4). The weight is dropped from the height $H = 500\,\text{mm}$ and the initial velocity of the weight, W, is chosen as $v = -3130\,\text{mm/s}$. Figures 6–9 show the results of analysis for the T-shaped joint of $l_2/l_1 = 0.4$ ($2l_1 = 50\,\text{mm}$, $2l_2 = 20\,\text{mm}$). Figure 6 shows the maximum principal stress propagation at the positions $x/l_1 = 0, 0.4, 0.8$ and 1.0 of the interface between the adherend and the adhesive ($y = -h_2/2$, $z = w$), where Young's modulus, E_1, and Poission's ratio, ν_1, of the adherends are 206 GPa and 0.3, respectively and those of the adhesive are $E_2 = 3.6$ GPa and $\nu_2 = 0.38$. The ordinate is the maximum principal stress, σ_1, and the

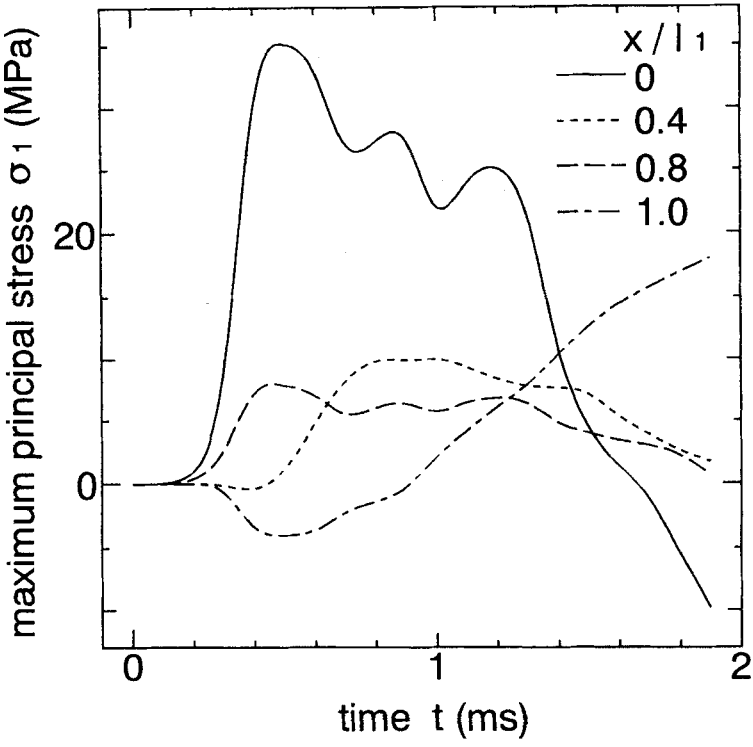

FIGURE 6 Maximum principal stress at the interface ($y = -h_2/2$, $z = w$) in the case of T-shaped joints ($l_2/l_1 = 0.4$, $h_2/h_1 = 0.0067$, $h_3/h_1 = 4$, $E_1/E_2 = 57$, $v = -3130$ mm/s).

abscissa is the time initiated. It is seen that the maximum principal stress, σ_1, becomes maximal at the center ($x/l_1 = 0$, $y = -h_2/2$, $z = w$) of the adherend to which the impact load is applied.

Figure 7 shows the maximum principal stress, σ_1, at the interface ($y = -h_2/2$, $z = w$) between the adhesive and the lower adherend (Solid 3 in Fig. 1) when the time initiated t is 0.3, 0.4, 0.5 and 0.6 ms. The maximum principal stress, σ_1, is found to be maximal at the center of the interface ($x/l_1 = 0$, $y = -h_2/2$, $z = w$) between the adhesive and the lower adherend. It is also seen that the maximum principal stress increases near the position $x/l_1 = 0.5 \sim 0.6$ due to the wave reflection at the flange end ($y = h_2/2 + h_1$). Figure 8 shows the maximum principal stress propagation at the interfaces of $y = -h_2/2$

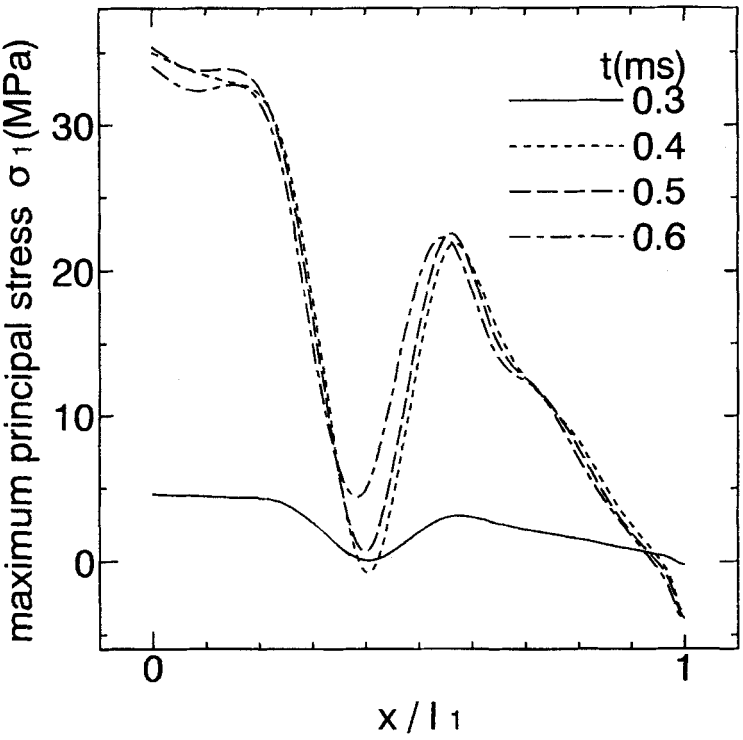

FIGURE 7 Maximum principal stress distributions at the interface ($y = -h_2/2$, $z = w$) in the case of T-shaped joints ($l_2/l_1 = 0.4$, $h_2/h_1 = 0.0067$, $h_3/h_1 = 4$, $E_1/E_2 = 57$, $v = -3130$ mm/s).

and $y = h_2/2$ ($x/l_1 = 0$, $z = w$) and at the center $y = 0$ ($x/l_1 = 0$, $z = w$) in the adhesive. It is indicated that the maximum principal stress, σ_1, becomes maximal at the interface ($x/l_1 = 0$, $y = -h_2/2$, $z = w$) of the lower adherend (Solid 3 in Fig. 1) to which the impact load is applied. From the result, it can be predicted that a rupture initiates from the interface of the lower adherend to which the impact load is applied. Figure 9 shows the propagation of stress components at the interface ($y = -h_2/2$, $z = w$) between the adhesive and the lower adherend when the time initiated, t, is 0.5 ms. It is found that the stress σ_y is the greatest while the normal stresses σ_x and σ_z are greater. These stresses, σ_x and σ_z, are thought to be Stoneley waves which propagate along the interface.

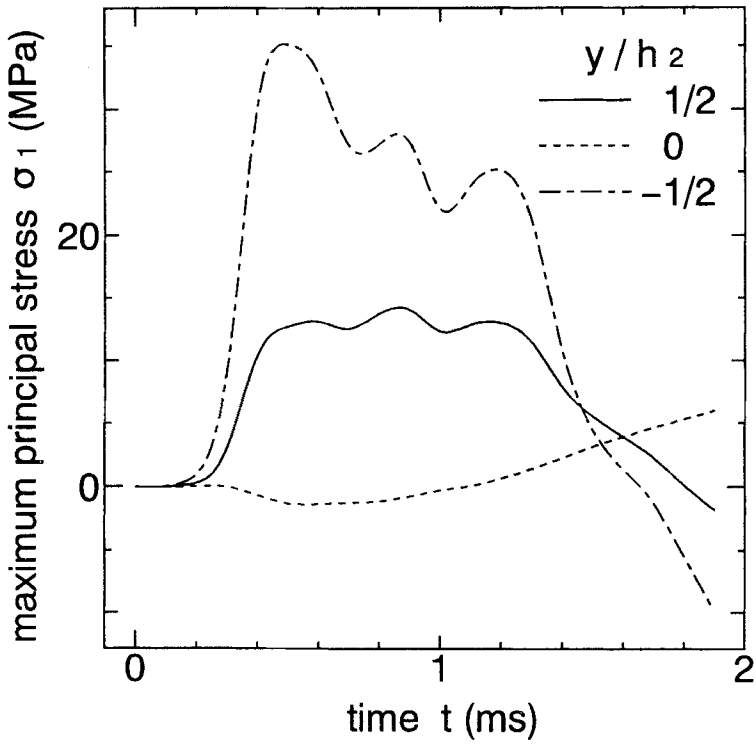

FIGURE 8 Maximum principal stress at the interface ($y = -h_2/2$, $h_2/2$) and at the middle of adhesive ($y = 0$) in the case of T-shaped joints ($l_2/l_1 = 0.4$, $h_2/h_1 = 0.0067$, $h_3/h_1 = 4$, $E_1/E_2 = 57$, $v = -3130$ mm/s).

Figures 10–13 show the results of analysis for the joints shown in Figure 3 when the web length $2l_2$ is equal to the flange length $2l_1$ and the initial velocity v(−626 mm/s) is one–fifth, in comparison with the results (Figs. 6–9) for the T-shaped joints shown in Figure 1. The rupture stress of the adhesive is supposed to be about 50 MPa. Thus, the height H is reduced to $H = 100$ mm in this joint. Figure 10 shows the maximum principal stress propagation at the positions $x = 0$, 0.4, 0.8 and 1.0 of the interface between the adhesive and the lower adherend. It is seen that the maximum principal stress, σ_1, becomes maximal at the edge ($x/l_1 = 1.0$) of the interface of the lower adherend to which the impact load is applied. Figure 11 shows the maximum principal stress, σ_1, at the interface ($y = -h_2/2$, $z = w$) between the

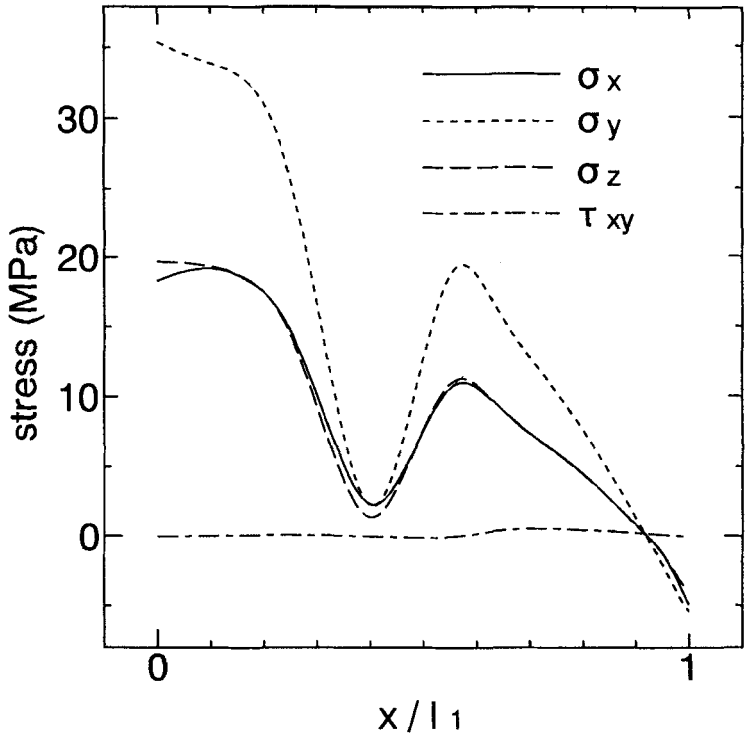

FIGURE 9 Each stress at the interface ($y = -h_2/2$, $z = w$) in the case of T-shaped joints ($l_2/l_1 = 0.4$, $h_2/h_1 = 0.0067$, $h_3/h_1 = 4$, $E_1/E_2 = 57$, $v = -3130$ mm/s, $t = 0.5$ ms).

adhesive and the lower adherend when the time initiated, t, is 0.5, 1.1 and 1.5 ms. When the time initiated, t, is 1.1 ms, the maximum principal stress, σ_1, becomes maximal at the edge of the interface ($x/l_1 = 1.0$, $y = -h_2/2$, $z = w$) and it seems to be singular.

Figure 12 shows the maximum principal stress propagation at the positions $y = -h_2/2$, $y = 0$ and $y = h_2/2$ of the edge ($x/l_1 = 0$, $z = w$). It is seen that the stress, σ_1, becomes maximal at the edge ($x/l_1 = 1.0$, $y = -h_2/2$, $z = w$) of the interface of the lower adherend to which the impact load is applied. Figure 13 shows the propagation of stress components at the interface ($y = -h_2/2$, $z = w$) between the adhesive and the lower adherend. Each stress component seems to be singular at the edge of the interface and the effect of the flange end which occurred in the T-shaped joint is not seen in this joint. Furthermore,

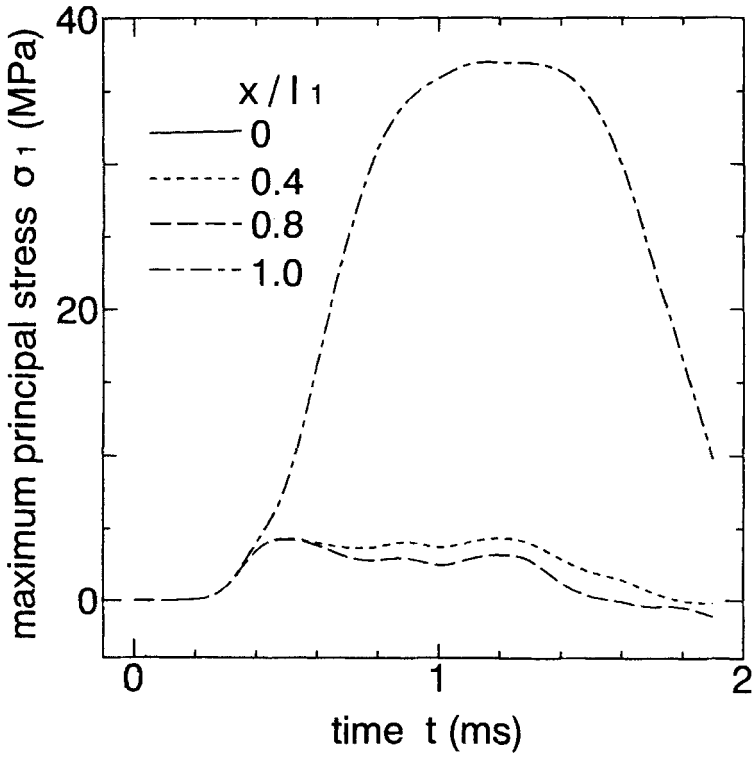

FIGURE 10 Maximum principal stress at the interface ($y = -h_2/2$, $z = w$) in the special case where web length $2l_2$ equals to flange length $2l_1$ ($l_2 = l_1$, $h_2/h_1 = 0.0017$, $E_1/E_2 = 57$, $v = -626$ mm/s).

it is noticed that the stress, σ_x, at the edge is the greatest while the stresses σ_z and σ_y are greater. The stresses σ_x and σ_z are thought to be Stonely waves which propagate along the interface. This result is different from the result for the *T*-shaped joint shown in Figure 9. In addition, it can be predicted that the maximum principal stress, σ_1, of joints ($v = -626$ mm/s, Figs. 10–13) shown in Figure 3 when the height of the weight is $H = 500$ mm is greater than that of the *T*-shaped joints ($v = -3130$ mm/s, Figs. 6–9) shown in Figure 1. Thus, it can be concluded that the strength of *T*-shaped joints is greater than that of joints where the web length is equal to the flange length.

Figure 14 shows the maximum principal stress propagation at the positions $x/l_1 = 0$, 0.3, 0.7 and 1.0 of the interface ($y = -h_2/2$, $z = w$)

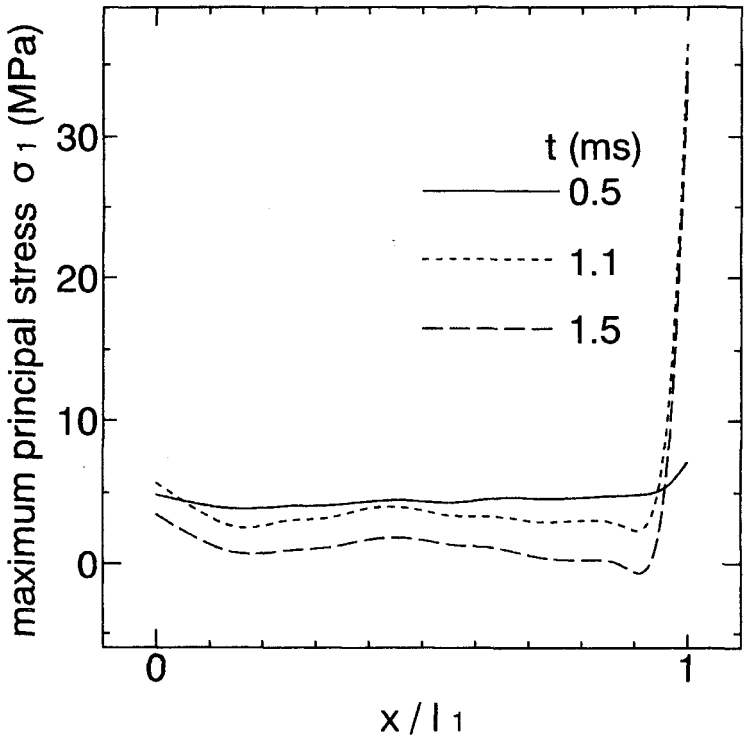

FIGURE 11 Maximum principal stress distribution at the interface ($y = -h_2/2$, $z = w$) in the special case ($l_2 = l_1$, $h_2/h_1 = 0.0017$, $E_1/E_2 = 57$, $v = -626$ mm/s).

between the adhesive and the lower adherend, where the ratio l_2/l_1 in the T-shaped adherends is 0.7 ($2l_1 = 50$, $2l_2 = 35$). The maximum principal stress, σ_1, is found to be maximal at the position of $x/l_1 = 0.3$ ($x = 7.5$ mm). From the comparison with the results in the case $l_2/l_1 = 0.4$ shown in Figure 6, it can be predicted that the position where the maximum principal stress σ_1 occurs moves from the center ($x/l_1 = 0$) toward the edge ($x/l_1 = 1.0$) of the interface ($y = -h_2/2$, $z = w$) between the adhesive and the lower adherend. In addition, it is seen that the maximum principal stress, σ_1, decreases as the ratio l_2/l_1 increases and it becomes maximal when the ratio l_2/l_1 is 1.0, that is, when the web length is equal to the flange length. In general, it is noticed that the stress waves propagate through the lower pin and the lower web shown in Figure 1 and they start to disperse at the flange

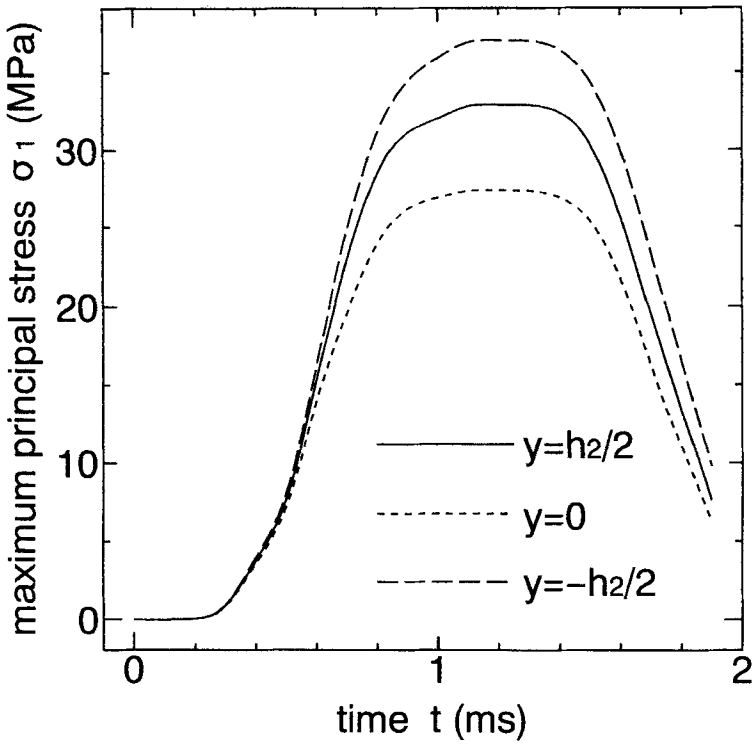

FIGURE 12 Maximum principal stress at the interface ($y = -h_2/2$, $z = w$) and at the middle of adhesion ($y = 0$) in the special case ($l_2 = l_1$, $h_2/h_1 = 0.0017$, $E_1/E_2 = 57$, $v = -626$ mm/s).

end ($y = h_2/2 + h_1$), which is the intersection between the web and the flange, and the reflections are repeated. Thus, it is supposed that the position where the maximum value of σ_1 occurs moves toward the edge of the interface due to the dispersive and the reflection effects at the flange end as the web length, l_2, increases. In addition, since the impacted load is the same, the propagated stress at the interface is decreased as the web length, l_2, increases. Thus, the maximum value of σ_1 is decreased as the web length, l_2, increases.

Figure 15 shows the maximum principal stress propagation at the lower interface ($y = -h_2/2$, $z = w$) when the time t is 0.4, 0.5 and 0.6 ms. The maximum principal stress, σ_1, is seen to be maximal at the position $x/l_1 = 0.3$ ($y = -h_2/2$, $z = w$) when the time t is 0.5 ms. In the

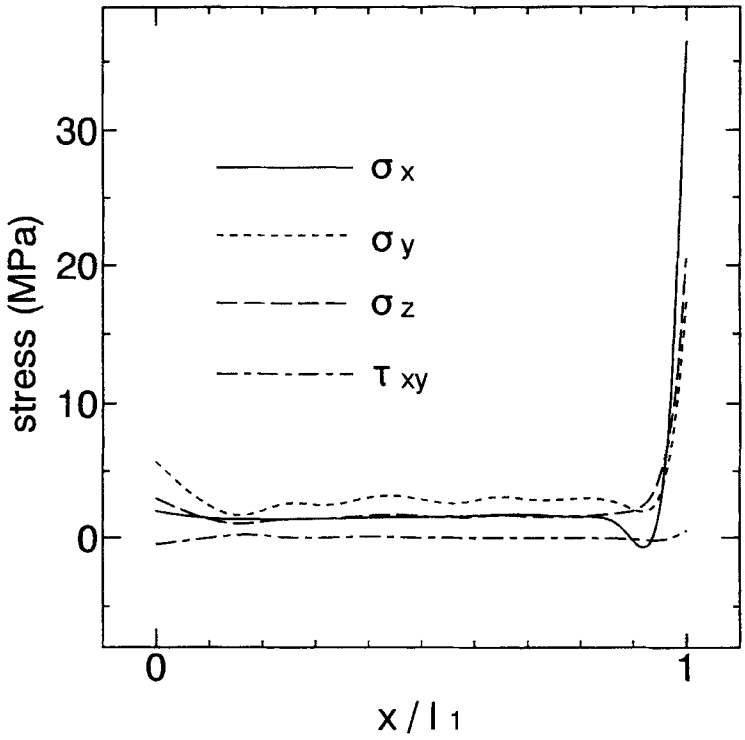

FIGURE 13 Each stress at the interface ($y = -h_2/2$, $z = w$) in the special case ($l_2 = l_1$, $h_2/h_1 = 0.0017$, $E_1/E_2 = 57$, $v = -626\,\text{mm/s}$, $t = 1.5\,\text{ms}$).

comparison with the case of Figure 11 (the case of $l_2 = l_1$), the time ($t = 0.5\,\text{ms}$) when the maximum value of σ_1 occurs is faster. It supposed that the maximum value of σ_1 occurs due to the dispersive and reflection effects at the flange end ($y = h_2/2 + h_1$) and the interface in the T-shaped joints because the stress component σ_y is the greatest in comparison with the Stoneley waves σ_x and σ_z. On the other hand, the dispersive effect does not occur in the case where the web length is equal to the flange length (Figs. $10 \sim 13$) and, thus, it is supposed that the time ($t = 1.1\,\text{ms}$) when the maximum value of σ_1 occurs is later than that ($t = 0.5\,\text{ms}$) in the T-shaped joints. In addition, the effect of the height, h_1, of the T-shaped joint shown in Figure 2 on the interface stress distribution is examined by changing the height, h_1, to 5, 15 and 60 mm. As a result, it is found that when the

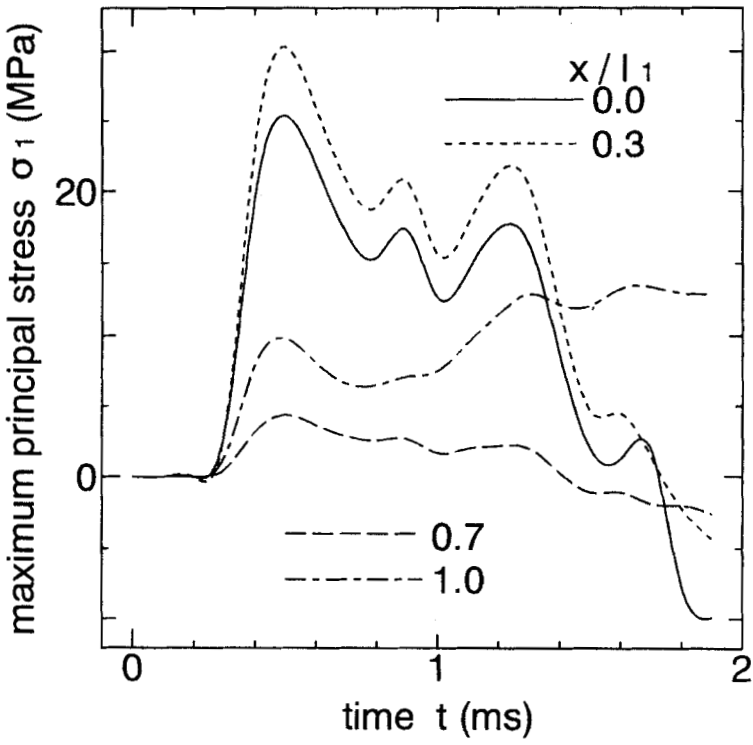

FIGURE 14 Maximum principal stress at the interface ($y = -h_2/2$, $z = w$) ($l_2/l_1 = 0.7$, $h_2/h_1 = 0.0067$, $h_3/h_1 = 4$, $E_1/E_2 = 57$, $v = -3130$ mm/s).

value of h_1 is 60 mm, the interface stress distribution is the same as that of the joint where the web length is equal to the flange length shown in Figures 10–13. When the value of h_1 is 60 mm in the T-shaped joint, the incident stress waves are seen to be approximately uniform in the lower adherend through the lower pin and the effect of the reflection at the flange end is thought to be small. Thus, it can be concluded that the effect of the flange in T-shaped joints is substantial.

Figure 16 shows the effect of Young's modulus ratio, E_1/E_2, between the adherend and the adhesive on the maximum principal stress, σ_1, at the position $x = 0$ of the lower interface ($y = -h_2/2$, $z = w$) when the ratio l_2/l_1 is 0.4 (T-shaped adherend shown in Fig. 4). It is seen that the maximum principal stress, σ_1, becomes maximal as the ratio E_1/E_2 increases. In addition, it is also found that the time when the maximum

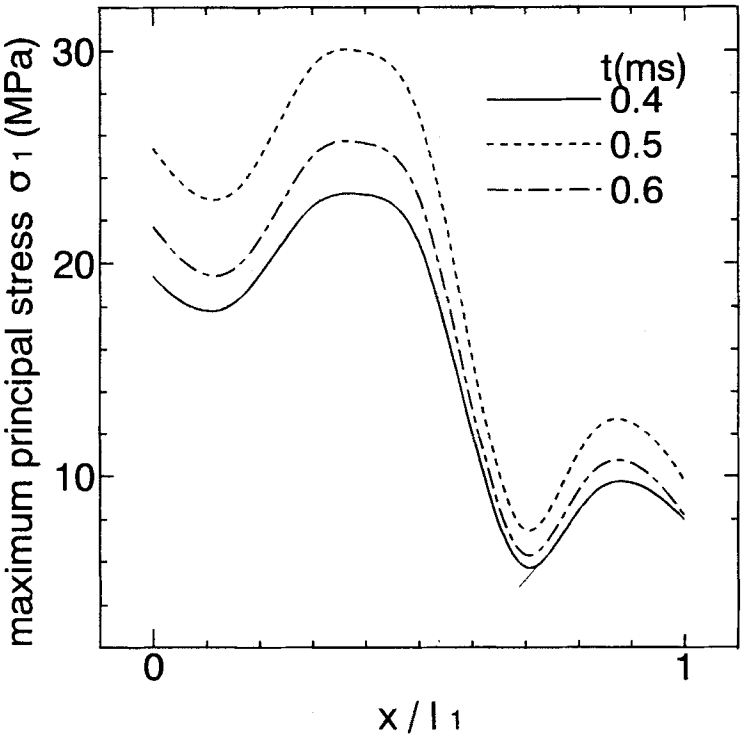

FIGURE 15 Maximum principal stress distributions at the interface ($y = -h_2/2$, $h_2/2$) ($l_2/l_1 = 0.7$, $h_2/h_1 = 0.0067$, $h_3/h_1 = 4$, $E_1/E_2 = 57$, $v = -3130$ mm/s).

value of σ_1 occurs is decreased. It is thought that the number of superimposed reflected stress waves is increased at the lower interface as Young's modulus E_1 increases because the velocity of the wave which propagates in the adherends increases (while Young's modulus E_2 is held constant) and, thus, the maximum stress increases and the time when the maximum value occurs is decreased.

Figure 17 shows the effect of Young's modulus ratio, E_1/E_2, on the maximum principal stress, σ_1, at the edge ($x/l_1 = 1$) of the lower interface ($y = -h_2/2$, $z = w$) when the ratio l_2/l_1 is 1.0; that is, when the web length is equal to the flange length (Fig. 3). It is seen that the maximum principal stress, σ_1, increases as the ratio E_1/E_2 decreases. This result is opposite to the result for the T-shaped joints shown in Figure 16. In this case of $l_2 = l_1$, Stoneley stress waves σ_x and σ_z which

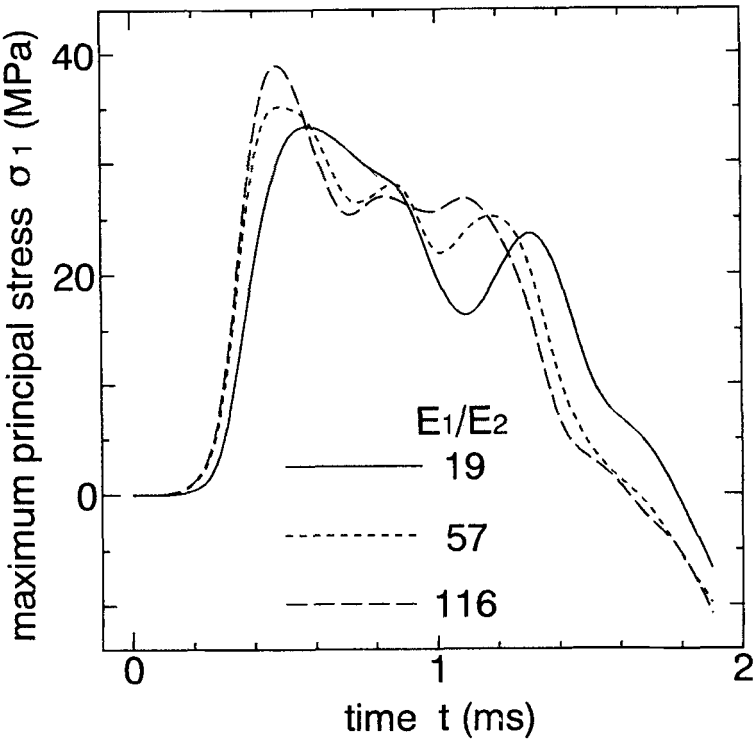

FIGURE 16 Effects of Young's modulus ratio E_1/E_2 on the maximum principal stress at the interface ($x = 0$, $y = -h_2/2$, $z = w$) in the case of T-shaped joints ($l_2/l_1 = 0.4$, $h_2/h_1 = 0.0067$, $h_3/h_1 = 4$, $v = -3130$ mm/s).

propagate along the interface are greater than the normal stress, σ_y, and they influence the maximum principal stress σ_1. In addition, it is supposed that Stoneley waves depend on Young's modulus ratio E_1/E_2 between the adherend and the adhesive and they increase as the ratio E_1/E_2 decreases ($E_1 \neq E_2$) due to the characteristics of Stonely waves.

Figure 18 shows the effect of the adhesive thickness ratio h_2/h_1 ($h_1 = 15$ mm in Fig. 4) on the maximum principal stress, σ_1, at the center ($x = 0$, $y = -h_2/2$, $z = w$) of the lower interface when the ratio l_2/l_1 in the T-shaped joint is 0.4 (Fig. 4). It is seen that the maximum value of the stress increases as the ratio h_2/h_1 increases. These results show the same tendency as those for the joints subjected to static tensile loads [5, 7]. Figure 19 shows the effect of the thickness ratio, h_2/h_1,

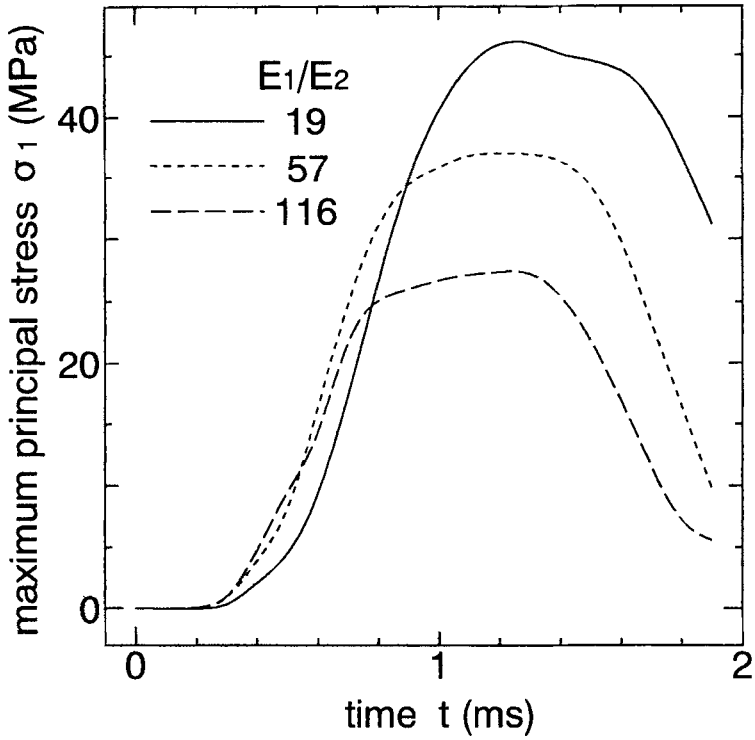

FIGURE 17 Effects of Young's modulus ratio E_1/E_2 on the maximum principal stress at the interface ($x = l_1$, $y = -h_2/2$, $z = w$) in the special case ($l_2 = l_1$, $h_2/h_1 = 0.0017$, $v = -626$ mm/s).

on the maximum principal stress, σ_1, at the edge ($x = l_1$, $y = -h_2/2$, $z = w$) of the lower interface when the web length is equal to the flange length, that is, the ratio l_2/l_1 is 1.0. It is seen that the maximum principal stress, σ_1, increases as the ratio h_2/h_1 increases. In Figure 19, it is seen that the time when the maximum value of σ_1 occurs is the same, independent of the adhesive thickness. In Figure 20, the same tendency is seen. From both the results shown in Figures 19 and 20, it can be supposed that the maximum value of σ_1 depends on the magnitude of the stresses σ_x and σ_z (Stoneley waves) and that these stresses increase as the adhesive thickness increases within the thickness range 20–30 μm.

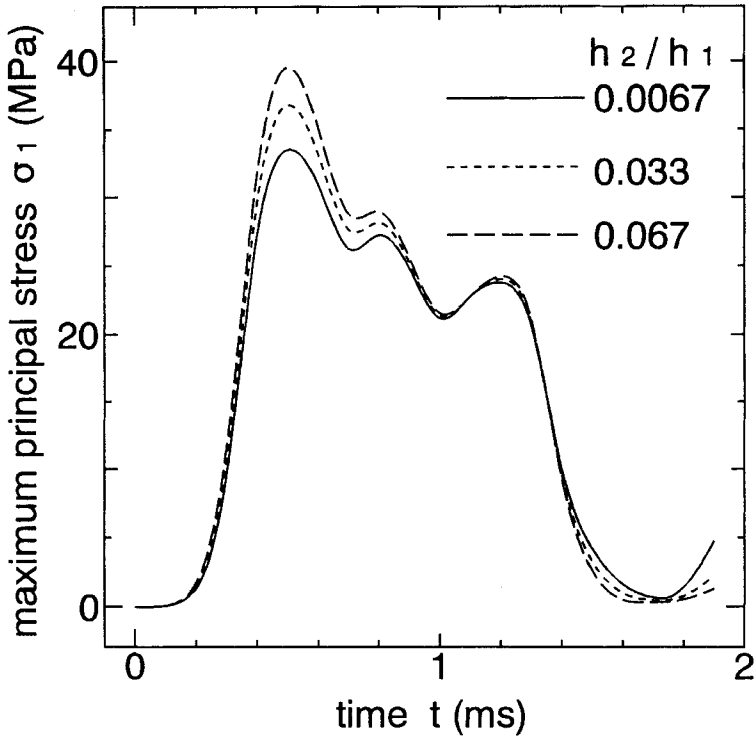

FIGURE 18 Effects of the thickness ratio h_2/h_1 on the maximum principal stress at the interface ($x = 0$, $y = -h_2/2$, $z = w$) in the case of T-shaped joints ($l_2/l_1 = 0.4$, $h_3/h_1 = 4$, $E_1/E_2 = 57$, $v = -3130$ mm/s).

Figure 20 shows the effect of the height, H, on the maximum principal stress, σ_1, at the center ($x/l_1 = 0$, $y = -h_2/2$, $z = w$) of the lower interface. It is seen that the maximum principal stress, σ_1, increases as the value of H increases. In addition, no difference in the tendency of the stress propagation is found. The maximum value of the principal stress, σ_1, is proportional to the value of H. The maximum value of the principal stress, σ_1, of the joint is calculated when the height H is changed to 0.1 mm in Figure 5. In addition, the maximum value of the principal stress, σ_1, of the joint subjected to a static load of 26.754 N shown in Figure 5 is analyzed in our previous paper [5]. It is found that the maximum value of the principal stress,

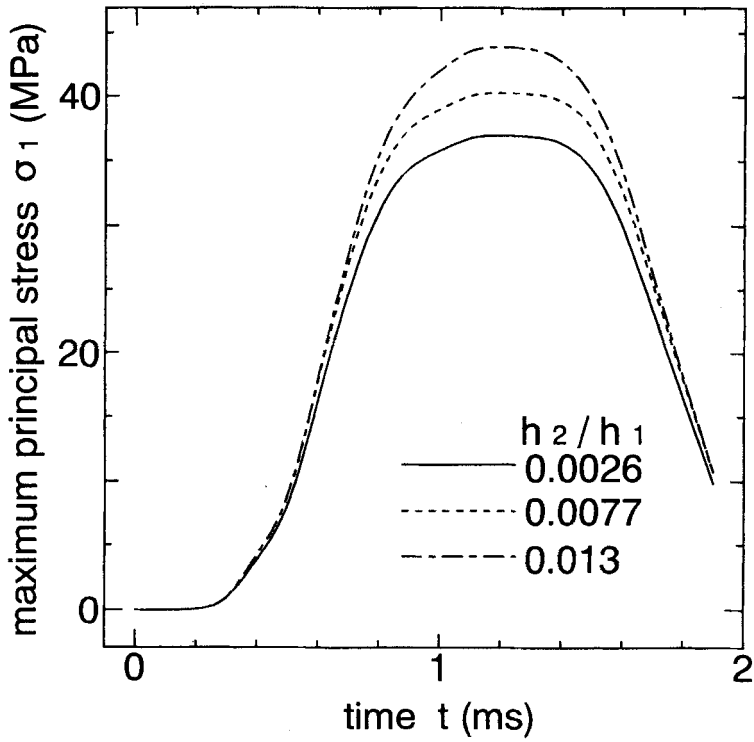

FIGURE 19 Effects of the thickness ratio h_2/h_1 on the maximum principal stress at the interface ($x = 0$, $y = -h_2/2$, $z = w$) in the special case ($l_2 = l_1$, $E_1/E_2 = 57$, $v = -626\,\text{mm/s}$).

σ_1, in the case when the value of H is 0.1 mm is about 4.2 times larger than that of a joint subjected to a static load [5].

4.2. Comparison between the Numerical and the Measured Results on the Strain Response

Figure 21 shows the comparison of the strain response. The strain response was measured at the positions of $x = 0$, 8, 12 and 16 mm shown in Figure 5. In Figure 21, the strain responses at the positions of $x = 0$ and 12 mm are indicated. The ordinate is the strain in the y-direction and the abscissa is the time. A fairly good agreement is seen between the numerical and the measured results.

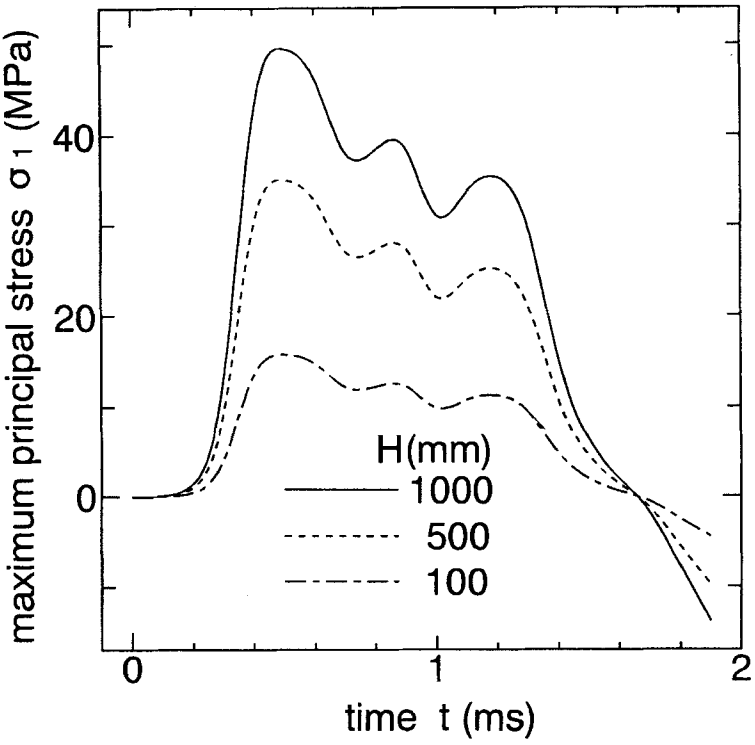

FIGURE 20 Effects of the dropping height, H, on the maximum principal stress at the interface ($x = 0$, $y = -h_2/2$, $z = w$) in the case of T-shaped joints ($l_2/l_1 = 0.4$, $h_2/h_1 = 0.0067$, $h_3/h_1 = 4$, $E_1/E_2 = 57$).

5. CONCLUSIONS

This paper dealt with stress response of adhesive butt joints subjected to impact load by using the FEM code DYNA3D. The results obtained are as follows.

(1) The maximum principal stress, σ_1, became maximal at the interface of the adherend to which the impact load was applied.
(2) The maximum value of the maximum principal stress, σ_1, in T-shaped joints moved from the center toward the edge of the lower interface and it decreased as the web length, $2l_2$, increased. In

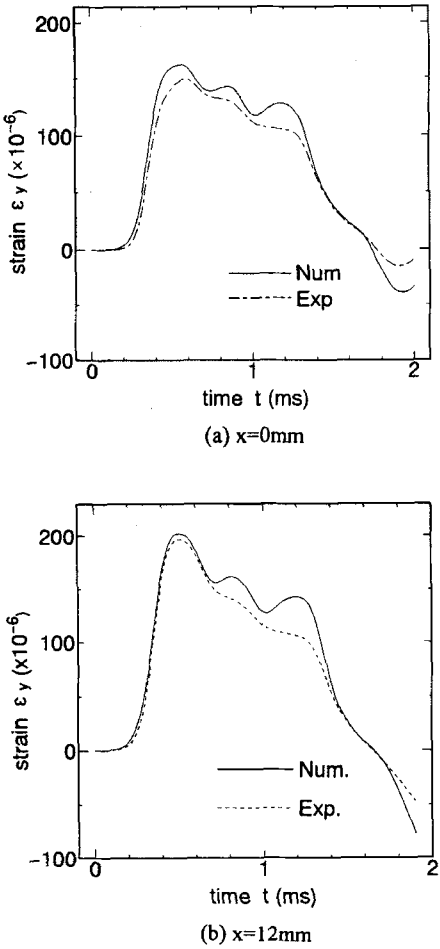

FIGURE 21 Comparison between the numerical and experimental results concerning strain response. (a) $x = 0$ mm (b) $x = 12$ mm.

addition, the maximum principal stress, σ_1, of a joint in the case when the web length, $2l_2$, was equal to the flange length, $2l_1$, was singular at the edge of the interface. In addition, it was found that the maximum value of the maximum principal stress, σ_1, was greater than that for the T-shaped joint when the drop height was the same.

(3) It was found that the maximum value of the maximum principal stress, σ_1, increased as the ratios E_1/E_2 and h_2/h_1 increased in the case of the *T*-shaped joints. In the case where the web length was equal to the flange length, the maximum value of σ_1 increased as the ratio E_1/E_2 decreased and the ratio h_2/h_1 increased.

(4) Strain measurements on adherends were carried out. A fairly good agreement was seen between the measured and the numerical results.

References

[1] Chen, Du., *J. Applied Mechanics* **57**, 78 (1990).
[2] Tsai, Ming-Yi and Morton, J., *J. Applied Mechanics* **61**, 712 (1994).
[3] Sawa, T., Nakano, Y. and Temma, K., *J. Adhesion* **24(1)**, 1 (1987).
[4] Shi, Y. P. and Cheng, S., *J. Engineering Mechanics* **119**(3), 584 (1993).
[5] Sawa, T., Temma, K., Nishigaya, T. and Ishikawa, H., *J. Adh. Sci. Technol.* **9**(2), 215 (1995).
[6] Sawa, T., Temma, K., Nishigaya, T., and Nakano, T., *Bull. JSME* **59**(563), 163 (1993).
[7] Temma, K., Sawa, T., Nishigaya, T. and Uchida, H., *JSME Int. J. Ser. A* **37**(3), 246 (1994).
[8] Nakagawa, F., Nakano, Y. and Sawa, T., *JSME Int. J. Ser. A* **37**(3), 238 (1994).
[9] Sawa, T., Senoo, Y., Okuno, H. and Hagiwara, T., *J. Adhesion* **59**, 1 (1996).
[10] Sato, T., Ito, T. and Ikegami, K., *Bull. JSME* **61**(590), 127 (1995).
[11] Sun, C. T. and Chattopadhyay, S., *J. Appl. Mech.* No. 75-WA/APM-10, p. 693 (1975).
[12] Xia, Y. and Ruiz, C., *IMechE* C387/005, 87 (1989).
[13] Zachary, L. W. and Burger, C. P., *Exp. Mech.* **20**, 162 (1980).
[14] Zhi-Hua ZHONG, *Finite Element Procedures for Contact-impact Problems*, Oxford Science Publications (1993).
[15] Hiroshima, T. and Sawa, T., *IMecE, J. Strain Anal.* **31**(1), 43 (1996).
[16] Hallquist, J. O., "User's Manuals for DYNA3D and DYNAP (Nonlinear Dynamic Analysis of Solids in Three Dimensions)", University of California, Lawrence Livermore National Laboratory, Reprint UCID-19156 (1981).
[17] Hallquist, J. O., "All Numerical Procedure for Three-dimensional Impact Problem", *American Society of Civil Engineering*, Reprint 2956 (1977).